Operating Frequency Prediction of Piezoelectric DC-DC converters

Lucas de Araujo Pereira, Adrien Morel, Mustapha Touhami, Theo Lamorelle, Ghislain Despesse, Gael Pillonnet

Operating Frequency Prediction of Piezoelectric DC-DC converters

Lucas de Araujo Pereira, Student Member, IEEE, Adrien Morel, Member, IEEE, Mustapha Touhami, Student Member, IEEE Théo Lamorelle, Ghislain Despesse, Gaël Pillonnet, Senior Member, IEEE

***Abstract*— Piezoelectric DC-DC converters operate between the series and parallel frequencies of the piezoelectric resonator to achieve soft switching and energy-balance conditions. This letter presents an experimentally validated model to accurately predict the operating frequency, the switching angles and the piezoelectric current for any 6-phases piezoelectric DC-DC converter. This model reduces the transient simulation's calculation time to reach steady state. It can be used to initially setup the switching angles in experiment, or to predict the high frequency spectrum generated by the converter cycle.**

Keywords*— *Piezoelectric resonator, operating frequency, mathematical model, DC-DC converter.

I. Introduction

Wide band-gap adoption among switching devices enables a drastic increase of the switching frequency in order to reduce the power converter size. However, the gain from high-frequency operation is mainly limited by the magnetic components' performances that scale sub-linearly with frequency [1]. In order to overcome the scaling limitations imposed by inductors, an emerging topology based on piezoelectric electromechanical resonators (PR) has been recently introduced in [2], then extended in [3]. As shown in Fig. 1.a, the PR DC-DC converter (PRC) is composed by arrangements of switching devices that allow adiabatic energy transfers through a DC-blocking PR. Promising experimental results show 10's W/cm^3 power density while maintaining high efficiency (>95%) at relatively low frequency (~100 kHz) [2, 3]. [2, 4] have already associated a self-tracking feedback to control each phase for sub-MHz operating range. [4, 5] have also proven the performance of the PR in MHz range, showing the capability to scale-down with frequency. [5, 10] points out the main performance criteria of PR converters: high electromechanical coupling and high mechanical quality factors. The mentioned challenges are mainly the control of switching instants at high frequency [4] and the reduction of spurious resonant modes [2, 5]. To help the designer to explore the PRC performance, an accurate prediction of switching cycle timing at early design stages is required.

In opposite to conventional converter structures, the cycle period of PR converters is fixed by the PR dynamics and electrical conditions. As shown in previous papers, the operating frequency (f) varies from series (f_s) to parallel (f_p) resonances PR frequencies ($f_p/f_s<1.3$), mainly dictated by the coupling factor [5]. The aforementioned papers make strong assumptions regarding the cycle period value to analytically approximate the converter's characteristics such as the power efficiency, or the piezoelectric current magnitude with tractable expressions. However, the precise cycle period enables to carefully size the PR, to accurately evaluate the piezoelectric current magnitude over a full power range, and to quantify the high frequency spectrum in order to avoid that some harmonics excite the higher PR resonance modes.

Based on a modelling approach adopted by the piezoelectric energy harvesting community for strong coupling PR [6, 7], this letter proposes to model the impact of the energy transfers (imposed by the converter topology) on the PR dynamics by adding an electrically induced capacitor C_e and negative resistor R_e (Fig. 1.b). Thanks to the well-known first harmonic approximation [6] and the Van Dyke PR model (input capacitance C_p in parallel with an *RLC* branch) [8, 9], this paper introduces a merged model combining the PR dynamics and the electrically-induced stiffness linked to the voltage across the PR, which is imposed by the PRC operation (Fig. 1.c). The coefficient α in the proposed merged model is derived from the frequency-spectrum decomposition of the piezoelectric voltage v_p mixed with the PR impedance.

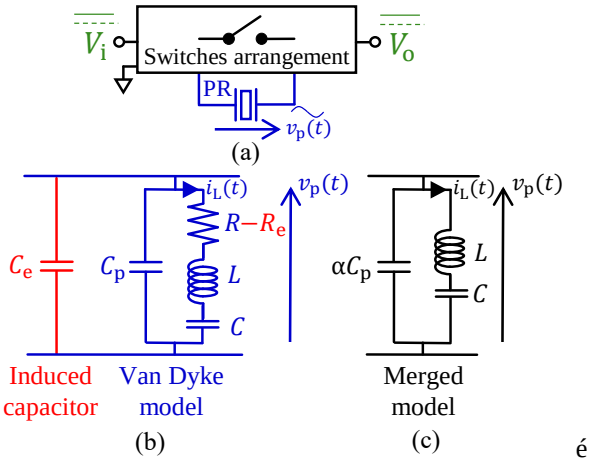

Fig. 1. (a) PR DC-DC converter, (b) electrically induced capacitor, and (c) merged model.

This letter describes how to calculate the coefficient α, the PR current amplitude I_m, the switching angles x_i [3] for any 6-phases PRC topologies. This method is applied to various PRC topologies used in previous articles [2, 4, 5] and proves that the proposed model is in good agreement with experimental results. Other benefits of this modelling are also discussed e.g. reaching the steady state faster, evaluating spurious modes effect.

II. Method Description

A. Operating principle and notations

The PRC operating principle is well described in [2-5]. To summarize and introduce the model's notations, this letter reminds some notions in this first section. The PRC is based on controlling the switching cycle (Fig. 2) synchronized with the PR oscillation by applying *Constant Voltage Phases* alternating with *Constant Charge Phases*, while ensuring both charges and energy balance [2, 3]:

1) Constant voltage phases (CVP): PR is connected to combinations of input, output and ground voltages, allowing the energy exchange between PR and voltage sources.

2) Constant charge phases (CCP): PR is open-circuited allowing a variation of the PR voltage $v_p(t)$ up to the value of the next CVP, enabling the soft swichting of the PRC.

A 6-phases cycle switching sequence is determined by:

- Three different CVP by cycle (V_1, V_3 and V_5), where V_3 and V_5 are located in the second half of the PR vibration period ($\forall x_i \in [\pi, 2\pi]$);
- Three different CCP by cycle (v_2, v_4 and v_6);
- At least one phase that is connected to each of the input voltage V_i and output voltage V_o;
- The voltages V_1, V_3 and V_5 can be equal to any linear combination of $\pm V_i$, $\pm V_o$ and zero.

For model genericity, the switching sequence is classified into two cases depicted in Fig. 2, where V_{max} and V_{min} are, respectively, the maximum and the minimum voltage values reached by $v_p(t)$. The coefficient z represents the initial phase of $i_L(t)$. Some sequences are given as example in Table I (K, μ_i are explained subsequently).

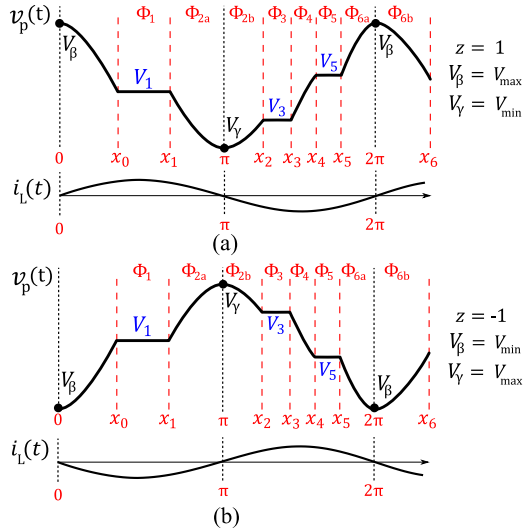

Fig. 2. (a) Generic form of v_p(t) and $i_L(t)$ of a 6-phases cycle with z=1. (b) Generic form of $v_p(t)$ and $i_L(t)$ of a 6-phases cycle with z=-1.

TABLE I. SWITCHING SEQUENCES PARAMETERS EXAMPLES

ref	Switching sequence			Voltage conversion	z	μ_1	μ_3	μ_5	K
	V_1	V_3	V_5						
[2]	V_i	0	V_o	$V_i < V_o$	1	0	0	1	$\frac{V_i}{2V_o}$
	V_o	V_i	0	$V_i > V_o$	-1	1	0	0	½
[3]	V_o	$V_i - V_o$	0	$V_i > 2V_o$	-1	1	1	0	$\frac{V_i}{2(V_i - V_o)}$
	$V_i - V_o$	0	V_o	$2V_o > V_i > V_o$	1	1	0	1	$\frac{V_i}{2V_o}$
[4]	V_o	$V_i - V_o$	$-V_o$	$0.5V_i > V_o$	-1	1	1	1	1
[5]	0	$V_i - V_o$	$-V_o$	$V_i > V_o$	-1	0	1	1	½

The switching sequence notation here is different from [3]. The phase reference on the waveform $i_L(t)$ is chosen (either Fig. 2(a) or Fig. 2(b)) in order to locate V_3 and V_5 in the second half of the PR vibration period ($\forall x_i \in [\pi, 2\pi]$). This phase reference is necessary for the model genericity for any 6-phases PRC topology.

B. Piezoelectric current amplitude

The PR current i_L is assumed to be purely sinusoidal with an amplitude I_m given by (1) for any switching sequence:

$$I_m = \pi\left(\frac{P_{out}}{2KV_o} + fC_p(V_{max} - V_{min})\right) \quad (1)$$

Where P_{out} is the transferred power, f the operating frequency and K is the charge utilization factor inspired in [3]. K can be calculated as the ratio between the CVP connected to the output and all the CVP:

$$K = \frac{\mu_1(V_3 - V_5) + \mu_3(V_1 - V_5) + \mu_5(V_3 - V_1)}{2(V_3 - V_5)} \quad (2)$$

Where μ_i is equal to 1 when the i^{th} phase is connected to the output and 0 otherwise (Table I).

C. Switching angles

The six switching angles have to be carefully fixed to allow soft switching operation, except x_3 (or x_4), which is the degree of freedom of the period that must be adjusted to achieve the desired P_{out} and V_o. From the general waveform given in Fig. 2, the duration of each phase is calculated relatively to the cycle period using the following equations:

$$x_0 = \cos^{-1}\left(1 + z\frac{(V_1 - V_\beta)}{A}\right) \quad (3)$$

$$x_1 = \cos^{-1}\left(-1 - z\frac{(V_\gamma - V_1)}{A}\right) \quad (4)$$

$$x_2 = \cos^{-1}\left(-1 + z\frac{(V_3 - V_\gamma)}{A}\right) \quad (5)$$

$$x_3 = 2\pi - \cos^{-1}\left(\frac{\theta_2 V_3 + V_5\left(z\frac{V_5 - V_3}{A} - \theta_5\right) - V_1(\theta_1 - \theta_0) + z(\pi R I_m)}{(V_3 - V_5)}\right) \quad (6)$$

$$x_4 = 2\pi - \cos^{-1}(\theta_3 + z\frac{(V_5 - V_3)}{A}) \quad (7)$$

$$x_5 = 2\pi - \cos^{-1}\left(1 - z\frac{(V_\beta - V_5)}{A}\right) \quad (8)$$

$$x_6 = 2\pi + x_0 \quad (9)$$

Where $A = I_m/(2\pi f C_p)$ and $\theta_i = \cos(x_i)$.

D. Fundamental of the voltage across PR

If the operating frequency f is assumed to be constant (equal to f_s or f_p as in [2, 3]), I_m and x_i can be analytically derived from (1) to (9). However, f varies between f_s and f_p inducing non-negligible errors. In practice, the operating frequency is found by adjusting manually the frequency and the switching angles until finding the ZVS operation like in [2] or by introducing self-synchronization blocks as in [3]. To calculate I_m and x_i precisely without any adjustment, this letter proposes the following method.

Considering that the PR exhibits a large quality factor and operates in steady state, the first harmonic approximation method (FHA) is applied in order to evaluate the impact of the fundamental harmonic of the piezoelectric voltage on the PR dynamics [6, 7]. The fundamental of the piezoelectric voltage $v_p(t)$ can be expressed as:

$$v_p(t)\big|_{n=1} = a_1\cos(2\pi f t) + b_1\sin(2\pi f t) \quad (10)$$

Where a_1 and b_1 are the firsts Fourier coefficients. Physically, they can be associated with an electrically induced stiffness (modifying the PR resonance frequency) and an electrically induced damping as identified later in (17, 18). We can calculate these coefficients for any 6-phases PRC:

$$a_1 = \sum_{k=0}^{2}\left\{z\frac{V_{k+1}}{\pi}(\sin x_{2k+2} - \sin x_{2k}) + \frac{I_m}{2\pi^2 f C_p}\left[\frac{x_{2k+2} - x_{2k+1}}{2} + \frac{\sin 2x_{2k+2} - \sin 2x_{2k+1}}{4} - \cos x_{2k+1}(\sin x_{2k+2} - \sin x_{2k+1})\right]\right\} \quad (11)$$

$$b_1 = \sum_{k=0}^{2}\left\{z\frac{V_{k+1}}{\pi}(\cos x_{2k} - \cos x_{2k+2}) + \frac{I_m}{\pi\omega C_p}\left[\frac{\cos 2x_{2k+1} - \cos 2x_{2k+2}}{4} - \cos x_{2k+1}(\sin x_{2k+1} - \sin x_{2k+2})\right]\right\} \quad (12)$$

Where x_i are the switching angles calculated with (3-9) and V_k is the CVP (V_1, V_3 and V_5).

E. Merged model

By applying mesh analysis to the PR equivalent Van Dyke model (Fig. 1(b)), (10) can be derived.

$$v_p(t) = L\frac{dq^2}{d^2t} + R\frac{dq}{dt} + \frac{1}{C}q \tag{13}$$

Since the current $i_L(t)$ and electric charge q are linked by (14), the expression of the charge is given by (15).

$$i_L(t) = I_m \sin(2\pi f t) = \frac{dq}{dt} \tag{14}$$

$$q = -\frac{I_m}{2\pi f}\cos(2\pi f t) \tag{15}$$

Based on the FHA, (10) can be combined with (13 – 15) to obtain the second order differential equation governing the charge transfer into the PR:

$$L\frac{d^2q}{dt^2} + \left(R - \frac{b_1}{I_m}\right)\frac{dq}{dt} + \left(\frac{1}{C} + \frac{a_1 2\pi f}{I_m}\right)q = 0 \tag{16}$$

The equation (16) can be identified as a RLC branch (Fig. 1(b)) including the PR Van Dyke model along with electrically induced components (C_e and R_e) due to the switching sequence at first harmonic. The electrically induced capacitor C_e and resistor R_e are deduced by:

$$C_e = \frac{I_m}{a_1 2\pi f} \tag{17}$$

$$R_e = \frac{b_1}{I_m} \tag{18}$$

In steady state operation, the PR is energy balanced over a complete switching sequence, thus the electrically induced resistor compensates the PR losses introduced by R:

$$R_e = \frac{b_1}{I_m} = -R \tag{19}$$

The averaged behavior over one cycle given by (16) can be represented as a merged model (Fig. 1(c)) by merging C_e into C_p using the coefficient α (20).

$$\alpha = \frac{I_m}{a_1 2\pi f C_p} \tag{20}$$

For sinusoidal steady state, the resonance frequency of the merged model can be obtained by solving (21).

$$(4\pi^2 LC)f^2 + (2\pi\frac{I_m}{a_1})f - 1 = 0 \tag{21}$$

The previous equations form a system:

$$\begin{cases} (1-2) \\ (3-9) \\ (11) \\ (21) \end{cases} \leftrightarrow \begin{cases} I_m = \mathrm{F}(f, P_{out}) \\ x_i = \mathrm{G}(I_m, v_p) \\ a_1 = \mathrm{H}(x_i, I_m, f, v_p) \\ f = \mathrm{J}(a_1, I_m) \end{cases} \tag{22}$$

The system (22) is not analytically solvable. Therefore, this system is numerically solved in order to find the operating frequency, the current amplitude I_m and x_i.

III. Experimental Validation

Two PRC topologies have been chosen to compare the proposed model to transient simulations and experimental results. The constant voltages V_1, V_3 and V_5 are given in Table I, for the step-down [4] and step-up [2] topologies, respectively. The PRC experimental setup are described in these two papers [2, 4], and the $PR_{1,2}$ parameters are shown in table II.

Figures 4 and 5 show, from experimental data, SPICE simulations, and the numerical solved system given by (22), the variation of the operating frequency (normalized by f_s) and coefficient α as a function of the output power for the two topologies ([4] and [2]). The model prediction matches the electrical simulations i.e. Δf_{max}=10 Hz, equivalent to 0.07% error on [f_p-f_s]. It gives a reasonable accuracy i.e. <1.5% error compared to the experimental results.

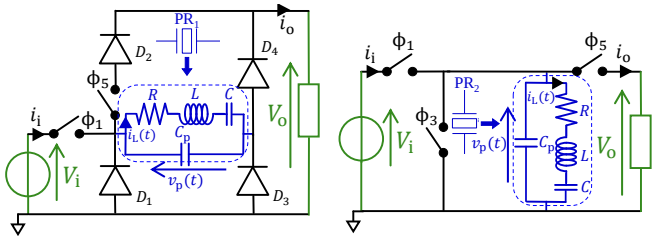

Fig. 3. PRC topologies used during the experimental model validation.

TABLE II. PARAMETERS OF THE PR USED DURING THE VALIDATION

PR	L	C	C_p	R	f_s	Q	k
PR_1	1.1 mH	2.9 nF	8.4 nF	0.4 Ω	89 kHz	1537	52%
PR_2				0.6 Ω		1025	

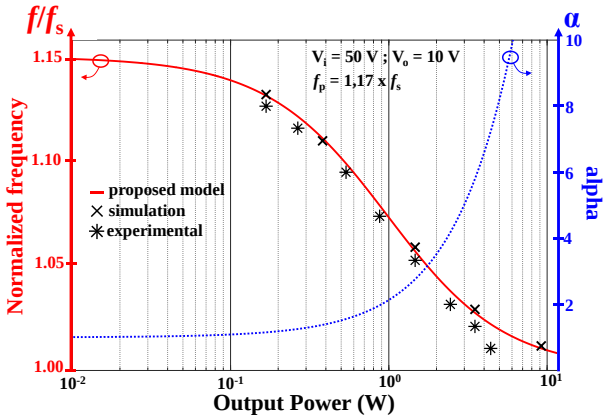

Fig. 4. Operating frequency vs the output power for sequence used in [4].

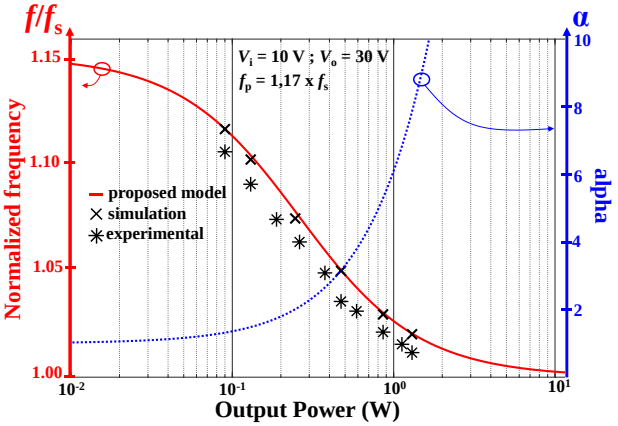

Fig. 5. Operating frequency vs the output power, for sequence used in [2].

A small deviation between the experimental curve and the theoretical and simulation curves is observed in Fig. 5 due to additional parasitic PR connection. For low power transfer, α tends to 1, meaning no capacitance is induced by the converter (C_e≈0), and the PR operates at its open-circuit resonance frequency (f=f_p). For high output power, α tends to infinity (C_e→+∞) as the converter cycle induces additional stiffness on PR, thus reducing the operating frequency.

IV. Discussions

A. Faster steady state convergence

To design an optimal PRC (e.g. sizing the switches or choosing a particular PR), several electrical simulations are needed. Reaching the steady state faster is a key enabler to perform sweep-simulations. The first method is to calculate the angles assuming a constant frequency (f=f_s), the targeted powers are not guaranteed and the PRC operates without ZVS. The second method is to numerically sweep the frequency between f_p and f_s to find the right angles, derived from (3) to (9), to reach soft switching and the targeted output power. Considering a 10 Hz frequency step (same accuracy as the proposed model), 1500 electrical simulations are required (1 hour of processing on a personal computer). Otherwise, this paper presents a third method that consists in determining the operating frequency and the angles x_i by calculation before running a single transient simulation (2.4 seconds of processing on a personal computer). Note that [3] proposes an alternative numerical method to find the frequency based on solving differential equations, but the authors have not enough details to include this method in this comparison.

Figure 6 illustrates efficiency over a range of output power for the three aforementioned methods. Anew, the proposed model is still validated to give fast and accurate results to reach the steady state. The pre-calculated initial conditions from the proposed model can also be used during experimentation in order to set the angles x_i, thus reducing the losses before reaching the effective steady state.

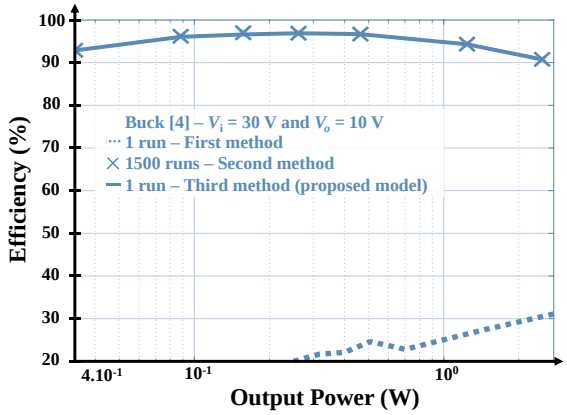

Fig. 6. Efficiency vs the output power, based on sequence [2].

B. Spurious mode prediction

[2] reports an efficiency drop-off due to higher resonant modes excitation (>f_p). To predict this issue at an early design stage, the other Fourier coefficients (a_i, b_i, i >1) can also be derived to predict the amplitude of the higher harmonics of v_p. Fig. 7 depicts the cumulative frequency spectrum and the total harmonic distortion (THD) across various output powers for the topology [2]. The proposed model predicts the frequencies and amplitude outside [f_s, f_p], then can be combined with PR impedance measurements in order to evaluate the effect of spurious modes.

[5] also reported the non-negligible effect of other resonance modes on the efficiency of PRC, especially those located between f_s and f_p. If the PR impedance is known at an early design stage, the accurate frequency prediction allowed by the proposed model can also be used to predict the limitations on the output power. In [5], when the switching sequence (V_i-V_o, 0, V_o) is tested with a voltage conversion from V_i=50 V to V_o=25 V, the minimum measured power output is equal to 18 W. Above this operating frequency (6.82 MHz), the unwanted vibration modes cause the efficiency to drop. Based on the proposed model and using the data provided in [5], 15.5 W is the minimum power output value in order not to excite higher resonance modes (which is relatively close to the 18 W reported in [5]). It is still a way to validate the proposed model and underline its genericity for any 6-phases PRC sequences.

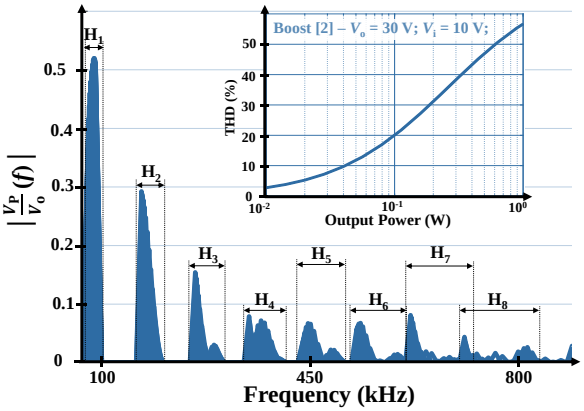

Fig. 7. Cumulative frequency spectrum from 0.01 to 1 W output power. and THD based on sequence [2] over output power.

V. Conclusion

This letter proposes a model to predict the operating frequency and switching angles accurately for any 6-phases PRC topology. The proposed model is based on an electrically-induced capacitor to emulate the effect of switching sequence of PRC. The model has been experimentally validated. The model can be used to reduce the calculation time for transient simulations or to quickly reach ZVS operation by setting the right steady state. The model is also valuable for predicting the high frequency spectrum generated by PRC on PR, and to evaluate the excitation of the PR higher resonance modes.

References

[1] C. R. Sullivan et al., "On size and magnetics: Why small efficient power inductors are rare, in *2016 International Symposium on 3D Power Electronics Integration and Manufacturing* (3D-PEIM), June 2016, pp. 1-23.

[2] B. Pollet, G. Despesse and F. Costa, "A New Non-Isolated Low-Power Inductorless Piezoelectric DC–DC Converter," *IEEE Transactions on Power Electronics*, vol. 34, no. 11, pp. 11002-11013, 2019.

[3] J. D. Boles, J. J. Piel and D. J. Perreault, "Enumeration and Analysis of DC–DC Converter Implementations Based on Piezoelectric Resonators," *IEEE Transactions on Power Electronics*, vol. 36, no. 1, pp. 129-145, 2021.

[4] M. Touhami, G. Despesse and F. Costa, "A New Topology of DC-DC Converter Based On Piezoelectric Resonator," *in 21st Workshop on Control and Modeling for Power Electronics*, 2020, pp. 1-7.

[5] W. D. Braun et al., "Optimized Resonators for Piezoelectric Power Conversion," *IEEE Open Journal of Power Electronics*, vol. 2, pp. 212-224, 2021.

[6] A. Morel, et al., "Frequency tuning of piezoelectric energy harvesters thanks to a shortcircuit synchronous electric charge extraction," *Smart Mater. Struct.*, vol. 28, no. 2, pp. 025009 1-14, 2019.

[7] J. Liang and W. Liao, "Impedance Modeling and Analysis for Piezoelectric Energy Harvesting Systems," in *IEEE/ASME Transactions on Mechatronics*, vol. 17, no. 6, pp. 1145-1157, Dec. 2012.

[8] K. S. Van Dyke, "The Piezo-Electric Resonator and Its Equivalent Network," *Proceedings of the Institute of Radio Engineers*, vol. 16, no. 6, pp. 742-764, June 1928.

[9] G. Ivensky, I. Zafrani, and S. Ben-Yaako, "Generic operational characteristics of piezoelectric transformers," IEEE Trans. on Power Electronics, vol. 17, no. 6, pp. 1049-1057, Nov. 2002.

[10] J. D. Boles, et al., "Evaluating Piezoelectric Materials for Power Conversion," *in 21st Workshop on Control and Modeling for Power Electronics*, 2020, pp. 1-8.